euronoise

An analysis of the modes of wave propagation in cylindrical shells

Yu-Cheng Liu[a], Yun-Fun Hwang[b] and Jin-Huang Huang[c]

[a]Graduate Institute of the Mechanical & Aeronautical Engineering, Feng Chia University, No. 100 Wenhwa Rd., Seatwen, 40724 Taichung, Taiwan
[b]Electroacoustic Graduate Program, No. 100 Wenhwa Rd., Seatwen, 40724 Taichung, Taiwan
[c]Department of Mechanical and Computer-Aided Engineering, No. 100 Wenhwa Rd., Seatwen, 40724 Taichung, Taiwan
p9245215@fcu.edu.tw

The dynamic stiffness method is proposed to examine the dispersion of waves in an inclusion-reinforced composite plate. The shape of inclusion is modelled as spheroid that enables the composite reinforcement geometrical configurations ranging from sphere to short and continuous fiber. Using the Mori-Tanaka mean-field theory, the effective elastic moduli of the composite plate are predicted explicitly and are able to elucidate the effect of inclusion's shape and volume fraction on the composite elastic behaviour. The resulting moduli are then applied to the dynamic stiffness matrix. From these findings indispensable information on the requirements for examining the dispersion of waves in the plate in vacuo are obtained. Numerical simulations have been given for dispersions in various wave types at various inclusion shape, inclusion content, and plate thickness as well. The results indicate that the inclusion content, aspect ratio and the plate thickness affect the propagation velocity and wavenumbers. Larger aspect ratios generally possess higher propagation speed. In other words, using short fibers generally results in a lower propagation speed.

1 Introduction

Information about the vibration and acoustic radiation characteristics of a solid structure may be obtained from its dispersion relation, which relates the angular frequency ω to the propagation wavenumber k. Some important characteristics readily seen from the dispersion relation are: (1) phase velocity, (2) group velocity, and (3) frequency range where the wave is able to propagate (*i.e.*, is not evanescent). The propagation velocity and wavelengths associated with the dispersion relation are directly related to the sound radiation efficiency of the structure. The corresponding eigenvector for each k will also provide the information about the modal structure and acoustic radiation characteristic of the propagating wave. Since only the transverse displacement of a plate produce sound, the relative magnitudes among the tangential, longitudinal, and transverse modal components are particularly important in structural acoustics. All of these important structural acoustics features can be obtained from a thorough analysis of the dispersion relation. Furthermore, the solution of a finite plate vibration under a specific boundary condition can also be obtained from the dispersion relation together with the associated eigenvectors, including all propagating and non-propagating (evanescent) modes. Such a dispersion relation has been a subject of great interest for several decades in various applications, including structural acoustics, non-destructive testing, noise control engineering, earthquake engineering, geotechnical engineering, material property identification, etc.

The characteristic analysis of sound radiation from an infinite plate has been investigated by authors [1-2] using either the classical thin plate or Timoshenko-Mindlin plate theory. It is well known that the classical thin plate theory is only applicable at frequencies much lower than the coincidence frequency where it predicts infinite flexural phase and group velocities. Using the Timoshenko-Mindlin plate theory has shown a considerable improvement of the classical theory, especially at and near the coincidence frequency [3]. Based on elasticity theory, several exact and numerical methods have been proposed to characterize waves in anisotropic [4-5] laminated plates. Among them, the method of dynamic stiffness is one of simple and powerful techniques for analyzing wave phenomena in layered media. This technique, as applied to acoustics, has its roots in the work of Pestell and James [6]. Spicer [7] developed a simple vector decomposition obtaining the dynamic stiffness matrix of an isotropic elastic layer. The most general analysis of this method was given by Skelton and James [8,9] and Hwang et al [10] to give a theoretical description of sound radiation from composite layered media. Their studies have facilitated both the exact and numerical solutions for acoustic radiation by a composite plate. In light of the simplicity of the dynamic stiffness method, the present work will employed this method to analyze wave dispersion in a fiber-reinforced composite plate in vacuo.

As fiber-reinforced composites gain popularity, the need for a basic understanding of the composites grows. This paper addresses acoustic radiation from fiber-reinforced composite plates made of a base material with stronger inclusions. The most essential material properties of such a composite are elastic constants, which govern the composite vibroacoustic behaviour. In this study, the Mori-Tanaka mean-field theory [11-12] is initially adopted to model an inclusion-reinforced composite and to elucidate the influence of inclusion aspect ratio and inclusion content on the overall elastic behavior. The inclusions are treated as spheroidal inclusions whose aspect ratio ranges from one (i.e., sphere) to much greater than one (i.e., continuous filament). Each constituent may be isotropic or anisotropic material. The resulting effective elastic constants of the plate then denotes as a function of phase properties, volume fraction, and inclusions' shape.

To analyze the dispersion relation of fiber-reinforced plates, the obtained effect elastic moduli are further applied to the dynamic stiffness matrix. From these findings indispensable information on the requirements for examining the vibroacoustic response of a laminated plate containing spheroidal inclusions in the plate in vacuo is obtained. Finally, numerical examinations for an E-glass/Epoxy inclusion-reinforced plate have been given. The information that how the volume inclusion fraction, the inclusion aspect ratio, and the plate thickness affect the propagation velocity and wavenumbers is clearly illustrated**.**

2 Effective elastic moduli of the composite plate

The study of wave dispersion in a composite plate inherently involves the estimation of their effective properties in terms of details of their microstructure, i.e., phase properties, volume fraction, shape, etc. As will be seen in the next section, the effective elastic properties are important and useful as they are the key ingredient necessary in the dynamic stiffness matrix for obtaining the wave dispersion in inclusion-reinforced composites. To

estimate the effective elastic properties, it is convenient to consider a sufficiently large composite plate containing identically shaped, unidirectionally aligned, and randomly distributed fibers with elastic moduli C^{1}_{ijmn} and volume fraction f. The domain surrounding the fibers is called matrix and has elastic moduli C^{0}_{ijmn}. Each fiber is approximated by a spheroidal inclusion defined by

$$\Omega : \frac{x_1^2}{a_1^2} + \frac{x_2^2 + x_3^2}{a_3^2} \le 1 \tag{1}$$

where a_1 and a_3 are the semiaxes of the spheroid. The assumption that the shape of fibers is spheroidal enables one to treat composite reinforcement geometries ranging from thin flake to continuous fiber reinforcement.

Based on the Huang's [12] previous results, the effective elastic moduli of fiber-reinforcement composites with unidirectionally aligned fibers can be written as

$$C_{ijmn} = C^{0}_{ijmn} + fC^{0}_{ijab}T^{-1}_{abqr}(C^{1}_{qrmn} - C^{0}_{qrmn}) \tag{2}$$

where T^{-1}_{abij} is the inverse of T_{abij} defined by

$$T_{ijab} = C^{0}_{ijab} + (1-f)(C^{1}_{ijmn} - C^{0}_{ijmn})S_{mnab} \tag{3}$$

with S_{mnab} being the well-known Eshelby tensors that can be found in the paper of Huang [13]. Throughout this paper, conventional indicial notation is used where repeated lowercase subscripts are summed over 1 to 3.

3 Dispersion of a thick orthotropic plate

The following derivation of the dispersion equation is based on the text of Skelton and James [9]. The strain components ε_{ij} are related to the displacement components u_i by the following relations.

$$\varepsilon_{ij} = \frac{1}{2}\left(\frac{\partial u_i}{\partial x_j} + \frac{\partial u_j}{\partial x_i}\right) \tag{4}$$

In the absence of body forces in the composite plate, the equations of motion are expressed as

$$\frac{\partial \sigma_{ij}}{\partial x_j} = \rho \frac{\partial^2 u_i}{\partial t^2} \tag{5}$$

For an orthotropic material, the constitutive equation that gives the following relation between stresses σ_{ij} and strains ε_{ij} is

$$\begin{Bmatrix} \sigma_{11} \\ \sigma_{22} \\ \sigma_{33} \\ \sigma_{23} \\ \sigma_{13} \\ \sigma_{12} \end{Bmatrix} = \begin{bmatrix} C_{11} & C_{12} & C_{13} & 0 & 0 & 0 \\ C_{12} & C_{22} & C_{23} & 0 & 0 & 0 \\ C_{13} & C_{23} & C_{33} & 0 & 0 & 0 \\ 0 & 0 & 0 & C_{44} & 0 & 0 \\ 0 & 0 & 0 & 0 & C_{55} & 0 \\ 0 & 0 & 0 & 0 & 0 & C_{66} \end{bmatrix} \begin{Bmatrix} \varepsilon_{11} \\ \varepsilon_{22} \\ \varepsilon_{33} \\ 2\varepsilon_{23} \\ 2\varepsilon_{13} \\ 2\varepsilon_{12} \end{Bmatrix} \tag{6}$$

where C_{ij} are the effective elastic constants given by equation (2). Denote the x_1x_2-spatial Fourier transform pairs of a field quantity $f(x_1,x_2,x_3)$ as

$$f(x_1,x_2,x_3) = \frac{1}{4\pi^2}\int_{-\infty}^{\infty}\int_{-\infty}^{\infty} f(\alpha,\beta,x_3)e^{\imath(\alpha x_1 + \beta x_2)}d\alpha d\beta \tag{7}$$

where $\imath = \sqrt{-1}$, α and β are the wave numbers for wave propagation in the x_1- and x_2-direction, respectively. Now, taking the x_1x_2-spatial Fourier transform of the time-harmonic equations of motion and with use of equations (4) and (6) leads to the following spectral equations of motion in wave number domain:

$$\left(\mathbf{X}\frac{\partial^2}{\partial x_3^2} + \imath\mathbf{Y}\frac{\partial}{\partial x_3} + \mathbf{Z}\right)\cdot\begin{Bmatrix} u_1(\alpha,\beta,x_3) \\ u_2(\alpha,\beta,x_3) \\ u_3(\alpha,\beta,x_3) \end{Bmatrix} = 0 \tag{8}$$

in which the coefficient matrices are given by

$$\mathbf{X} = \begin{bmatrix} C_{55} & 0 & 0 \\ 0 & C_{44} & 0 \\ 0 & 0 & C_{33} \end{bmatrix}$$

$$\mathbf{Y} = \begin{bmatrix} 0 & 0 & \alpha(C_{13}+C_{55}) \\ 0 & 0 & \beta(C_{23}+C_{44}) \\ \alpha(C_{55}+C_{13}) & \beta(C_{44}+C_{23}) & 0 \end{bmatrix}$$

$$\mathbf{Z} = \begin{bmatrix} -\alpha^2C_{11} - \beta^2C_{66} + \omega^2\rho & -\alpha\beta(C_{12}+C_{66}) & 0 \\ -\alpha\beta(C_{66}+C_{12}) & -\alpha^2C_{66} - \beta^2C_{22} + \rho\omega^2 & 0 \\ 0 & 0 & -\alpha^2C_{55} - \beta^2C_{44} + \rho\omega^2 \end{bmatrix} \tag{9}$$

To solve the spectral equations of motion (8) a solution in the form of the travelling waves:

$$u_i(\alpha,\beta,x_3) = U_i(\alpha,\beta)e^{\imath\gamma x_3} \tag{10}$$

is assumed, where γ is a wavenumber along the x_3 direction. Substituting the foregoing equation into equation (8) gives the following:

$$\begin{bmatrix} P_{11} + C_{55}\gamma^2 & P_{12} & P_{13}\gamma \\ P_{12} & P_{22} + C_{44}\gamma^2 & P_{23}\gamma \\ P_{12}\gamma & P_{23}\gamma & P_{33} + C_{33}\gamma^2 \end{bmatrix}\begin{Bmatrix} U_1(\alpha,\beta) \\ U_2(\alpha,\beta) \\ U_3(\alpha,\beta) \end{Bmatrix} = 0 \tag{11}$$

where

$$\begin{aligned} &P_{11} = \alpha^2C_{11} + \beta^2C_{66} - \rho\omega^2,\ P_{12} = \alpha\beta(C_{66}+C_{12}) \\ &P_{13} = \alpha(C_{13}+C_{55}),\ P_{22} = \alpha^2C_{66} + \beta^2C_{22} - \rho\omega^2 \\ &P_{23} = \beta(C_{23}+C_{44}),\ P_{33} = \alpha^2C_{55} + \beta^2C_{44} - \rho\omega^2 \end{aligned} \tag{12}$$

For a nontrivial solution, the determinant of the square symmetric matrix in equation (12) must be zero, thus yielding the characteristic equation

$$a_0\gamma^6 + a_1\gamma^4 + a_2\gamma^2 + a_3 = 0 \tag{13}$$

where the coefficients are given as

$$\begin{aligned} a_0 &= C_{55}C_{44}C_{33} \\ a_1 &= C_{44}(P_{11}C_{33} + P_{33}C_{55} - P_{13}^2) + C_{55}(C_{33}P_{11} - P_{23}^2) \\ a_2 &= P_{22}(P_{33}C_{55} + P_{11}C_{33}) + P_{11}P_{33}C_{44} - P_{11}P_{23}^2 \\ &\quad + 2P_{12}P_{23}P_{13} - P_{12}^2C_{33} - P_{13}^2P_{22} \\ a_3 &= P_{11}P_{22}P_{33} - P_{12}^2P_{33} \end{aligned} \tag{14}$$

Since the square matrix in equation (11) is positive definite, all of the resulting eigenvalues γ^2 are real and positive. Therefore, the six values of γ which satisfy the equation (13) are thus

$$\gamma_1 = +z_1,\ \gamma_2 = -z_1,\ \gamma_3 = +z_2$$
$$\gamma_4 = -z_2,\ \gamma_5 = +z_3,\ \gamma_6 = -z_3 \tag{15}$$

When these roots are substituted back into equation (11), we will obtain the six wave solutions (eigenvectors) $U_{iJ}(\alpha,\beta)$. Hereafter lowercase subscripts take on the range *1*, *2*, *3*, while uppercase subscripts range from *1* to *6*.

With the six wavenumbers and corresponding eigenfunctions, the spectral displacement solution can be constructed as a linear combination of six partial wave solutions:

$$u_i(\alpha,\beta,x_3) = \sum_{J=1}^{6} A_J U_{iJ}(\alpha,\beta) e^{\imath\gamma_J x_3} \tag{16}$$

where A_J are undetermined coefficients. This equation can be evaluated at the upper boundary ($x_3=h$) and the lower boundary ($x_3=0$), in turn, to give the matrix equation:

$$\mathbf{u}(\alpha,\beta) = \mathbf{rA} \tag{17}$$

where

$$\mathbf{u}(\alpha,\beta) = \{u_1(\alpha,\beta,h)\ \ u_2(\alpha,\beta,h)\ \ u_3(\alpha,\beta,h)$$
$$u_1(\alpha,\beta,0)\ \ u_2(\alpha,\beta,0)\ \ u_3(\alpha,\beta,0)\}^T$$

$$\mathbf{A} = \{A_1\ \ A_2\ \ A_3\ \ A_4\ \ A_5\ \ A_6\}^T \tag{18}$$

and the components of the coefficient matrix $\mathbf{r}$ are

$$r_{1J} = U_{1j}(\alpha,\beta)e^{i\gamma_J h},\qquad r_{2J} = U_{2J}(\alpha,\beta)e^{i\gamma_J h}$$
$$r_{3J} = U_{zJ}(\alpha,\beta)e^{i\gamma_J h},\qquad r_{4J} = U_{1J}(\alpha,\beta) \tag{19}$$
$$r_{5J} = U_{2J}(\alpha,\beta),\qquad r_{6J} = U_{3J}(\alpha,\beta)$$

Similarly, the relationship between the components of traction normal to the plate surfaces and the unknown coefficients can be also obtained:

$$\boldsymbol{\sigma}(\alpha,\beta) = \mathbf{pA} \tag{20}$$

where

$$\boldsymbol{\sigma}(\alpha,\beta) = \{\sigma_{31}(\alpha,\beta,h)\ \ \sigma_{32}(\alpha,\beta,h)\ \ \sigma_{33}(\alpha,\beta,h)$$
$$\sigma_{31}(\alpha,\beta,0)\ \ \sigma_{32}(\alpha,\beta,0)\ \ \sigma_{33}(\alpha,\beta,0)\}^T$$

and the elements in the matrix $\mathbf{p}$ given in the equation (20) are

$$p_{1J} = \imath C_{55}\left[\gamma_J U_{1J}(\alpha,\beta) + \alpha U_{3J}(\alpha,\beta)\right]e^{\imath\gamma_J h}$$
$$p_{2J} = \imath C_{44}\left[\gamma_J U_{2J}(\alpha,\beta) + \beta U_{3J}(\alpha,\beta)\right]e^{\imath\gamma_J h}$$
$$p_{3J} = \imath\left[\alpha C_{13}U_{1J}(\alpha,\beta) + \beta C_{23}U_{2J}(\alpha,\beta) + \gamma_J C_{33}U_{3J}(\alpha,\beta)\right]e^{\imath\gamma_J h}$$
$$p_{4J} = \imath C_{55}\left[\gamma_J U_{1J}(\alpha,\beta) + \alpha U_{3J}(\alpha,\beta)\right]$$
$$p_{5J} = \imath C_{44}\left[\gamma_J U_{2J}(\alpha,\beta) + \beta U_{3J}(\alpha,\beta)\right] \tag{21}$$
$$p_{6J} = \imath\left[\alpha C_{13}U_{1J}(\alpha,\beta) + \beta C_{23}U_{2J}(\alpha,\beta) + \gamma_J C_{33}U_{3J}(\alpha,\beta)\right]$$

The unknown vector $\mathbf{A}$ may be eliminated between equations (17) and (20), which results in

$$\mathbf{D}(\alpha,\beta)\mathbf{u}(\alpha,\beta) = \boldsymbol{\sigma}(\alpha,\beta) \tag{22}$$

where

$$\mathbf{D}(\alpha,\beta) = \mathbf{pr}^{-1} \tag{23}$$

is termed as the dynamic stiffness relating the spectral displacements and the spectral tractions at the boundaries. The quantities α, β, and ω are related by a dispersion relation, which gives the relationship between frequency and wavenumber. When the plate is free from surface tractions at the boundaries, equation (22) becomes

$$\mathbf{D}(\alpha,\beta)\mathbf{u}(\alpha,\beta) = \mathbf{0} \tag{24}$$

The dispersion relation is obtained by setting the determinant of the dynamic stiffness matrix $\mathbf{D}(\alpha,\beta)$ in the above equation equal to zero. This relationship displays the characteristic dispersive nature of wave propagation in the plates. That is, waves of different frequencies travel at different phase velocities. The resulting roots (the values of α and β) of the determinant of $\mathbf{D}(\alpha,\beta)$ characterize the free propagating waves, $u_i(\alpha,\beta,x_3)e^{\imath(\alpha x_1+\beta x_2)-\imath\omega t}$, in the plate. In this study, the focus is on the plane wave propagating along the x_1-axis only, that is, $u_i(\alpha,0,x_3)e^{\imath\alpha x_1-\imath\omega t}$.

4 Numerical results and discussions

In order to demonstrate how the volume fraction f and the aspect ratio a_1/a_3 of fibers affect the composite moduli and wave dispersion in the composite plate, following are discussed the numerical results for an E-Glass/Epoxy composite. The elastic properties used for the calculations are $C^0_{11}=8.23(GPa)$, $C^0_{12}=4.24(GPa)$ and mass density =1400 kg/m^3 for Epoxy matrix; $C^l_{11} = 83.34(GPa)$, $C^l_{12} = 23.51(GPa)$ and mass density =2800 kg/m^3 for E-Glass fibers. For this numerical simulation of the fiber-reinforced composite plate, fibers are oriented in the x_1 direction. In other words, the composite plate is reinforced primarily in the x_1 direction. By substituting the above values of C^0_{ij} and C^l_{ij} into equation (2), one finds that the nonzero terms are C_{11}, $C_{12}=C_{13}$, $C_{22}=C_{33}$, C_{23}, C_{44}, and $C_{55}=C_{66}$. It can be proved that $C_{44}=(C_{33}-C_{23})/2$, thus the composite includes only five independent elastic constants. This indicates that x_2x_3-plane is the plane of isotropy and the composite is macroscopically homogeneous and transversely isotropic.

Figure 2 shows the variations of the effective moduli C_{ij} with changes in the fiber aspect ratio a_1/a_3 at the fiber content $f=0.3$. It is illustrated that except C_{11}, all other moduli slightly decrease with the inclusion aspect ratio and have no apparent change when the ratio is greater than four. The figure also depicts that the influences of the inclusion aspect ratio on the Poisson's terms (C_{12} and C_{23}), transverse and shear moduli (C_{22} and C_{55}) are not as perceptible as the longitudinal modulus C_{11}. Figure 3 displays the effective moduli C_{ij} increase in a monotonic manner with respect to the fiber content f at the fiber aspect ratio a_1/a_3=64. For the material system studied herein, all effective moduli increase in a monotonic way with the fiber content f since the elastic constants of the fibers are stiffer than those of the matrix. Among the five independent moduli, the longitudinal modulus C_{11} increases significantly with f since the fibers are aligned and parallel to the x_1-axis. This suggests that the effects of the inclusion aspect ratio and volume fraction on the wave dispersion in the composite plate may be directly assessed based on C_{11}.

Figures 4 and 5 show the dispersion curves for the inclusion aspect ratio a_1/a_3=1 and 64, respectively, when the plate thickness is doubled (h=6 cm). The essential feature of the dispersion curve of this thicker plate are about the same as those of h=3 cm plate discussed above. However, thicker plates contribute smaller wave number than do thinner

plates. As can be seen in the figure, bending wave begins to be perceptible as the plate becomes thicker. It is worth noting that higher-order modes emerge at high frequencies. These modes are supersonic in both air and water. They are concerned primarily in ultrasonic and will be discussed in the future work. As usual, the first higher mode starts at frequency 10 kHz where the shear wave wavelength is two times the plate thickness and the corresponding wavenumber $k=2\pi/\lambda_{SH}=52.36$. The second higher mode starts at frequency 18 kHz where the plate thickness equals one half of the longitudinal wave wavelength, *i.e.*, $\lambda_L \doteqdot 12$ cm. Figure 4 also indicates that all waves in the thicker plate are supersonic in air. At frequencies below 16.5 kHz, the longitudinal wave is supersonic in water and becomes subsonic above 16.5 kHz and then gradually approaches to shear wave. For the same thickness plate with the aspect ratio $a_1/a_3=64$, the bending wave is close to the shear wave as indicated in Figure 5. The longitudinal wave is supersonic in water in all frequency intervals and its wave speed is much faster than that in Figure 4.

Figure 6 shows the variation of dispersion curves with the inclusion aspect ratio for the case $f=0.3$, $h=3$ cm, and $C^I_{11}/C^0_{11}=100$. It can be seen that bending and longitudinal wavenumbers decrease with the aspect ratio, while the shear wavenumber has no apparent change with the ratio. At the aspect ratio $a_3/a_1 =64$ all wavenumbers closely approach to their asymptotic values, indicating that the reinforcing effect due to fiber length is saturated at this value. Figure 7 illustrates the dispersion curves for various values of stiffness ratio C^I_{11}/C^0_{11}. The variation trends of the bending and shear behaviour with respect to different values of C^I_{11}/C^0_{11} closely resemble those in Figure 6. The stiffness ratio effect is found to be even more prominent for the longitudinal wave and the highest effect occurs at $C^I_{11}/C^0_{11}=100$.

5 Conclusion

The dynamic stiffness method presented here successfully solves the problems of the dispersion of waves in a composite plate reinforced with spheroidal inclusions. The effective moduli of the composite plate, appearing in the dynamic stiffness matrix, are predicted by the Mori-Tanaka mean-field theory. Use of the proposed method has demonstrated the capability of a straightforward continuous tracking on the changes of the dispersion relations and the corresponding modal patterns with frequency for each branch of the dispersion curves associated with a particular analytical root. Therefore, a parallel display of the dispersion curves used in this paper has shown to be useful to gain more insightful understanding about the wave phenomena in inclusion-reinforced composite plates.

Analysis results indicate that among the independent elastic moduli, the longitudinal modulus C_{11} parallel to fibers' direction is a dominant term, whereas the others are less influential. At high aspect ratio, the corresponding larger C_{11} (than the other moduli) results in much stronger bending stiffness, and the bending wave speed thus become greater. As the plate becomes thicker, bending waves begins to be perceptible and higher-order modes emerge at high frequencies, but shear and longitudinal wavenumbers are insensitive to thickness. Results also show that as the inclusion content f increases, bending and shear wavenumbers are significantly decreased, while longitudinal wavenumbers drop slowly.

In the future work, the effects by fluid-loading will be investigated. The approach used here will be modified to include the fluid-loading effect on the dispersion relations and the associated modal patterns in composite plates.

Acknowledgments

The author would like to thank the National Science Council of Taiwan, Republic of China, for the support of this research (NSC 95-2221-E-035-013-MY3 and 95-2221-E-035-087).

References

[1] Thompson, Jr., W., and Rattayya, J. V., "Acoustic Power Radiated by an Infinite Plate Excited by a Concentrated Moment", *J. Acoust. Soc. Am.*, 36, 1488–1490 (1964)

[2] Crighton, D. G., and Innes, D., "Low-Frequency Acoustic Radiation and Vibration Response of Locally Excited Fluid Loaded Structures", *J. Sound Vib.*, 91, 293–314 (1983)

[3] Junger, M. C., and Feit, D., "Sound, Structures, and Their Interactions", *Acoustical Society of America, American Institute of Physics* (1993)

[4] Y. F. Hwang, M. Kim, and P. J. Zoccola, "Acoustic radiation by a point- or line-excited laminated plates", *Journal of Vibration and Acoustics*, 122, 189-195 (2000)

[5] W.Q. Chen, H.M. Wang, and R.H. Bao, "On calculating dispersion curves of waves in a functionally graded elastic plate", *Composite Structures*, 81, 233-242 (2007)

[6] J.L. Pestle and James, "Sound radiation from layer media", *Admiralty Marine Technology Establishment, Teddington, Middlesex, AMTE(N)-TM79423* (1979)

[7] W.J. Spicer, "Free-wave propagation in and sound radiation by layer media with flow", *Admiralty Marine Technology Establishment, Teddington, Middlesex, AMTE(N)-TM82102* (1982)

[8] E.A. Skelton and J.H. James, "Acoustics of anisotropic planar layer media", *Journal of Sound and Vibration*, 152(1), 157-174 (1992)

[9] E.A. Skelton and J.H. James, "Theoretical Acoustics of Underwater Structures", *Imperial College Press* (1997)

[10] Hwang, Y.F., Kim, M., and Zoccola, P.J., "Acoustic radiation by point- or line-excited laminated plates", *Journal of Vibration and Acoustics*, 122, 189-195 (2000)

[11] Mori, T. and K. Tanaka, "Average Stress in Matrix and Average Energy of Materials with Misfitting Inclusions", *Acta Mettallurgica*, 21, 571-574 (1973)

[12] Huang, J.H., "Some Closed-form solutions for effective moduli of composites containing randomly

oriented short fibers", *Materials Science and Engineering A*, 315(1), 11-20 (2001)

[13] Huang, J.H. and Kuo, W.S., 1997, "The analysis of piezoelectric/piezomagnetic composite materials containing ellipsoidal inclusions", *Journal of Applied Physics*, 81(3), 1378-1386 (1997)

Figures

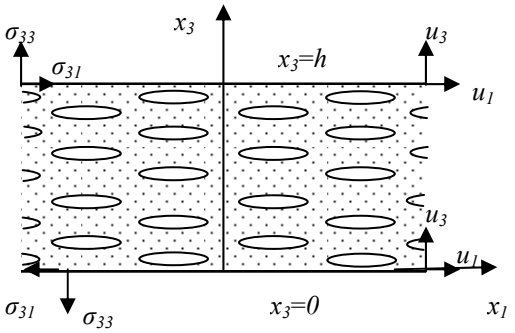

Fig.1 Geometry of a composite plate.

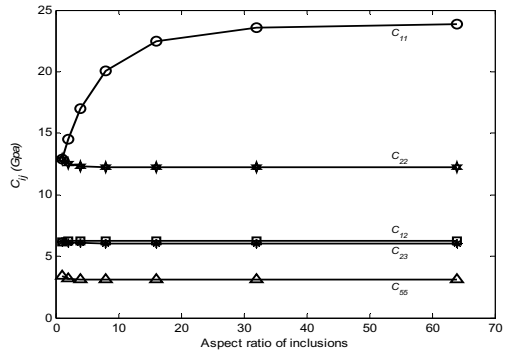

Fig.2 Effective moduli C_{ij} versus aspect ratio a_1/a_3 at inclusion content $f = 0.3$.

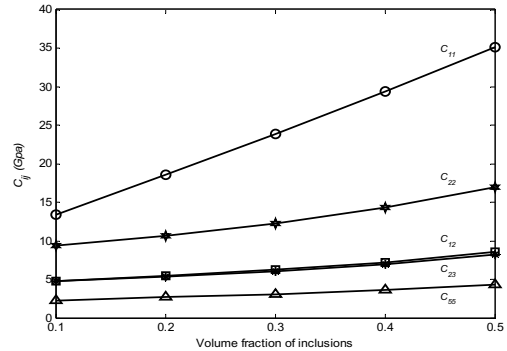

Fig.3 Effective moduli C_{ij} versus inclusion content f at aspect ratio a_1/a_3=64.

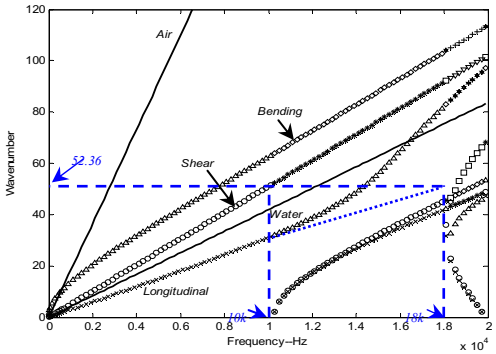

Fig.4 Dispersion curves for a 6 cm thick plate in vacuo at inclusion aspect ratio a_1/a_3=1.

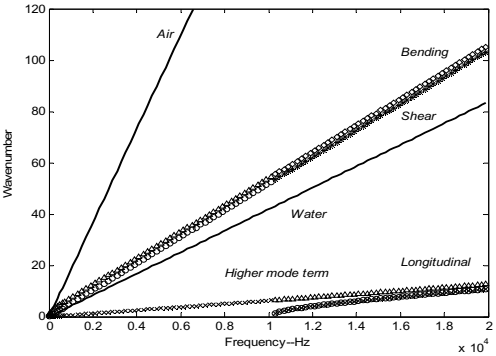

Fig.5 Dispersion curves for a 6 cm thick plate in vacuo at inclusion aspect ratio a_1/a_3=64.

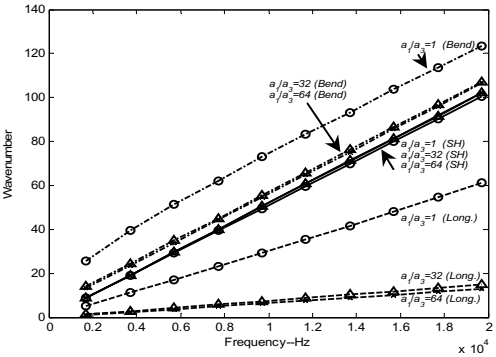

Fig.6 The effect of inclusion aspect ratio (a_1/a_3) variation on dispersion curves for a 3 cm thick plate in vacuo with C^1_{11}/C^0_{11}=100 and f=0.3.

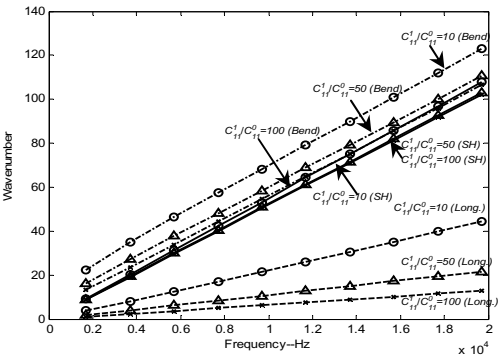

Fig.7 The effect of stiffness ratio (C^1_{11}/C^0_{11}) variation on dispersion curves for a 3 cm thick plate in vacuo with C^1_{11}/C^0_{11}=100 and f=0.3.